Feasibility analysis of an epidermal glucose sensor based on time-resolved fluorescence

Kamal M. Katika and Laurent Pilon*

Mechanical and Aerospace Engineering Department, Henry Samueli School of Engineering and Applied Science, University of California, Los Angeles, Los Angeles, California 90095, USA

*Corresponding author: pilon@seas.ucla.edu

Received 13 November 2006; revised 9 February 2007; accepted 13 February 2007; posted 13 February 2007 (Doc. ID 77024); published 15 May 2007

The goal of this study is to test the feasibility of using an embedded time-resolved fluorescence sensor for monitoring glucose concentration. Skin is modeled as a multilayer medium with each layer having its own optical properties and fluorophore absorption coefficients, lifetimes, and quantum yields obtained from the literature. It is assumed that the two main fluorophores contributing to the fluorescence at these excitation and emission wavelengths are nicotinamide adenine dinucleotide (NAD)H and collagen. The intensity distributions of excitation and fluorescent light in skin are determined by solving the transient radiative transfer equation by using the modified method of characteristics. The fluorophore lifetimes are then recovered from the simulated fluorescence decays and compared with the actual lifetimes used in the simulations. Furthermore, the effect of adding Poissonian noise to the simulated decays on recovering the lifetimes was studied. For all cases, it was found that the fluorescence lifetime of NADH could not be recovered because of its negligible contribution to the overall fluorescence signal. The other lifetimes could be recovered to within 1.3% of input values. Finally, the glucose concentrations within the skin were recovered to within 13.5% of their actual values, indicating a possibility of measuring glucose concentrations by using a time-resolved fluorescence sensor.

OCIS codes: 170.3660, 170.3650, 170.6920, 260.2510, 170.1470.

1. Introduction

There has been a rising interest in noninvasive glucose sensors based on fluorescence. Currently, diabetic patients measure their blood glucose concentrations by finger-prick capillary blood sampling, which is painful and prevents detection of abnormal glucose levels while sleeping or driving, for example. Therefore noninvasive and continuous glucose sensing is a priority in diabetes care [1].

Biological tissues contain several endogenous fluorophores such as nicotinamide adenine dinucleotide (NAD)H, aromatic amino acids like tryptophan, and structural proteins such as collagen and elastin [2]. Moreover, exogenous fluorescing substances can be applied to the skin or implanted within. The properties of these fluorophores are sensitive to the environment and the metabolic status of the tissue, thus making fluorescence spectroscopy a potential tool for continuously monitoring glucose concentrations in a minimally invasive manner. For example, implantable fluorescent sensors have been proposed for monitoring glucose concentrations in diabetic individuals [3,4]. These sensors would consist of a layer of fluorescent microspheres made out of a biocompatible polymer hydrogel implanted in the skin between the epidermis and the dermis. The fluorescence intensity emitted by these fluorophores is sensitive to glucose concentration, and thus the interstitial fluid glucose concentration could be monitored [5]. However, intensity-based measurements are sensitive to fluorophore concentration and to the intensity of the fluorescence signal [6], which in turn depends on the optical geometry and other factors such as skin complexion. On the other hand, fluorescence lifetimes are independent of fluorophore concentration and of the fluorescence intensity [7]. DiCesare and Lakowicz [6] synthesized fluorescence probes whose lifetimes are sensitive to the concentrations of glucose *in vitro* [6]. However, while there is a clear

0003-6935/07/163359-10$15.00/0

relationship between fluorescence lifetimes of the sensor and glucose concentrations *in vitro*, it might not be the case *in vivo*. Indeed, due to the presence of endogenous fluorophores in the skin, it might be harder to recover the fluorescence lifetime of the sensor from the overall fluorescence signal and thus determine the glucose concentration.

Therefore, the objective of the present study is to numerically test the feasibility of a noninvasive glucose sensor implanted under the skin and based on time-resolved fluorescence. This is achieved by modeling the time-resolved fluorescence from human skin by solving the transient radiative transfer equation. To the best of our knowledge, these simulations represent the first attempt to model time-resolved fluorescence from human skin using the radiative transfer equation. Moreover, it presents the first numerical feasibility study of implanted sensors based on time-resolved fluorescence.

2. Current State of Knowledge

Both experimental and numerical studies have been performed for time-resolved fluorescence measurements in turbid media and tissue. The reader is referred to Ref. 2 and references therein for a review of experimental studies. This review section is limited to numerical studies of time-resolved light transport and fluorescence in biological tissue.

One of the most common numerical tools used to study reflectance and fluorescence in biological tissue is the Monte Carlo method [8–11]. The main advantage of the Monte Carlo method resides in its simplicity and ability to deal with complex problems with relative ease. However, it requires a statistically meaningful number of photons and hence can be time consuming. The Monte Carlo technique has been used by Vishwanath *et al*. [12] to simulate time-resolved fluorescence from semi-infinite homogeneous turbid media. It was shown that the recovered lifetimes increased with increasing scattering and source–detector distance. This increase in lifetime was in good agreement with those seen in experiments simultaneously performed on tissue-simulating phantoms. The authors then applied the Monte Carlo method [13,14] to model data obtained from clinical measurements of fluorescence due to NADH and collagen in the lower gastrointestinal tract. The tissue was modeled as a two-layer medium with the top layer containing NADH as the fluorophore with a lifetime of 1.5 ns and the bottom layer containing collagen as a fluorophore with a lifetime of 5.2 ns. They investigated the effects of various parameters such as the tissue thickness, quantum yield, and absorption coefficient of the tissue on the fluorescence decay curves obtained. In addition, they showed numerically that measurements of the average fluorescence lifetime can be affected significantly in semi-infinite and inhomogeneous turbid media by fluorophore properties other than intrinsic lifetimes, such as fluorophore spatial distribution and concentration. Significant variations in the recovered average lifetimes were observed by changing the tissue morphology or factors related to tissue biochemistry in the numerical simulations while keeping the fluorescence lifetimes constant. These variations were comparable with the differences seen in the average lifetimes obtained from experiments on normal tissue and adenomatous polyps [13,14].

Alternatively, the diffusion approximation has been used extensively to simulate transient fluorescence transport in turbid media. For example, Patterson and Pogue [15] used it to predict the fluorescence photon fluence rate from semi-infinite tissue. The diffusion approximation was also used by O'Leary *et al*. [16] and Sevick-Muraca and co-workers [17,18] for fluorescence lifetime imaging in two-dimensional turbid media. While the diffusion approximation has been widely used to simulate radiation transport in biological tissue, it cannot be applied to all types of tissue. Various authors have shown that the diffusion approximation is not valid for highly absorbing tissue as well as tissue with a large scattering asymmetry factor [19,20].

As mentioned earlier, there has been a rising interest in noninvasive glucose sensors based on fluorescence. However, there are several issues in designing a glucose sensor based on time-resolved fluorescence, including (i) determining the optimal excitation and emission wavelength ranges of the fluorophore, (ii) finding the ideal range for the exogenous fluorophore lifetime, and (iii) relating the fluorophore lifetimes observed *in vivo* to the fluorophore lifetimes of the sensor and thus to the glucose concentration. The fluorophore should have an emission wavelength such that its fluorescence is not obscured by autofluorescence from the skin. Past studies [21,22] performed on steady-state spectral autofluorescence from skin and identifying the fluorescence excitation and emission bands from skin can address this question. Moreover, the sensor fluorophore lifetime has to be different from the fluorescence lifetime of endogenous fluorophores present in the skin. On the other hand, the relationship between measured fluorescence lifetimes of a sensor implanted in the skin and the glucose concentration has not been dealt with and is a part of this study. First, a model of skin fluorophores is constructed by using experimental data available in the literature. The hemispherical time-resolved fluorescence from human skin with and without an implanted glucose sensor is then obtained by solving the transient radiative transfer equation, using the modified method of characteristics [23,24]. Next, the fluorescence lifetimes are recovered from these decays by using Fluofit [25,26] and are compared with the actual lifetimes of the fluorophores used in the simulations. An attempt is then made to determine the glucose concentrations on the basis of the recovered fluorescence lifetimes.

3. Analysis

A. Skin Morphology

Skin is a complex biological structure made of multiple layers with different morphologies and optical properties. The topmost layer of the skin is the so-

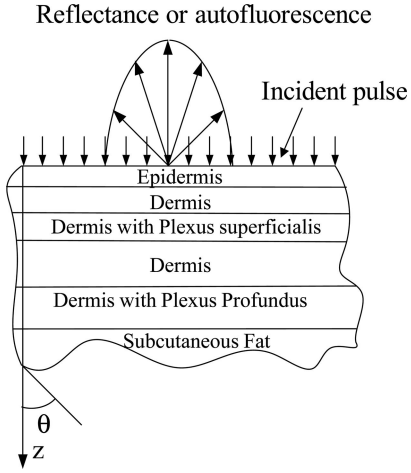

Fig. 1. Geometry of excitation and detection of reflectance and autofluorescence used in the simulations.

called *stratum corneum* and is composed of mainly dead cells embedded in a lipid matrix. The layer below is the *epidermis* and consists of cells containing keratohyalin granules, columnar cells, and other cells containing melanosomes and small melanin granules [27,28]. The third major layer of the skin is called the *dermis* and is primarily made up of collagen fibers with nerves and blood vessels running through. The dermis is sometimes divided into the *papillary dermis* and the *reticular dermis* on the basis of the size of their blood vessels [29]. All these layers add up to a thickness of about 2 mm [30]. Finally, there is the subcutaneous layer beneath the dermis, which consists of fat [10]. Figure 1 schematically shows the skin morphology and the excitation and detection configuration adopted in the present study.

Let us consider an area of skin exposed to monochromatic excitation light with wavelength λ_x. The excitation source could be an UV flashlamp, an ultrashort pulse laser, or a light-emitting diode (LED). The excitation light as it travels through the skin is then scattered or absorbed. Moreover, some absorbers such as proteins in the skin are known to fluoresce when excited at particular wavelengths. When a fluorescence-based sensor is embedded between the epidermis and the dermis, it will also contribute to the overall absorption, scattering, and fluorescence from the skin. The overall fluorescence signal from both the skin and the sensor can be transported to a detector by means of a strategically placed optical guide. If one assumes that the field of illumination is wider than the skin thickness, the problem can be treated as one dimensional [21]. Moreover, the detector is assumed to be of point size and to have a field of view of the entire hemisphere.

B. Governing Equations

The governing equation describing the transport of light in skin is the so-called transient radiative transfer equation (RTE) [31]. Even though it is a complex integrodifferential equation involving seven variables, it is preferred to the diffusion approximation for the reasons discussed previously. For absorbing, scattering, and nonemitting media at the excitation wavelength λ_x, the RTE can be expressed as [31]

$$\frac{1}{c_{\lambda_x}}\frac{\partial I_{\lambda_x}(\mathbf{r},\,\hat{\mathbf{s}},\,t)}{\partial t}+(\hat{\mathbf{s}}\cdot\nabla)I_{\lambda_x}(\mathbf{r},\,\hat{\mathbf{s}},\,t)=-\mu_{a,\lambda_x}I_{\lambda_x}(\mathbf{r},\,\hat{\mathbf{s}},\,t)-\mu_{s,\lambda_x}I_{\lambda_x}(\mathbf{r},\,\hat{\mathbf{s}},\,t)+\frac{\mu_{s,\lambda_x}}{4\pi}\int_{4\pi}I_{\lambda_x}(\mathbf{r},\,\hat{\mathbf{s}}_i,\,t)p_{\lambda_x}(\hat{\mathbf{s}}_i,\,\hat{\mathbf{s}})\mathrm{d}\omega_i, \tag{1}$$

where $I_{\lambda_x}(\mathbf{r},\hat{\mathbf{s}},t)$ is the excitation intensity in direction $\hat{\mathbf{s}}$ at location $\mathbf{r}$ and time t, and μ_{a,λ_x} and μ_{s,λ_x} are the linear absorption and scattering coefficients at the excitation wavelength, respectively. The scattering phase function $p_{\lambda_x}(\hat{\mathbf{s}}_i,\hat{\mathbf{s}})$ represents the probability that radiation propagating in the solid angle $\mathrm{d}\omega_i$ around direction $\hat{\mathbf{s}}_i$ will be scattered into the solid angle $\mathrm{d}\omega$ around direction $\hat{\mathbf{s}}$. The speed of light in the medium at the excitation wavelength is denoted by c_{λ_x} and is given by $c_{\lambda_x}=c_0/n_{\lambda_x}$, where c_0 is the speed of light in vacuum and n_{λ_x} is the local refractive index. The first and second terms on the right-hand side represent attenuation of the radiation intensity represented by absorption and scattering, respectively. The last term corresponds to the augmentation of radiation due to in scattering. Note that here the emission by the skin at 37 °C at the excitation wavelength λ_x is negligible compared with the excitation intensity.

Moreover, a similar equation can be written for the transport of the fluorescent light emitted by the fluorophores at the emission wavelength λ_F [2,32],

$$\frac{1}{c_{\lambda_F}}\frac{\partial I_{\lambda_F}(\mathbf{r},\,\hat{\mathbf{s}},\,t)}{\partial t}+(\hat{\mathbf{s}}\cdot\nabla)I_{\lambda_F}(\mathbf{r},\,\hat{\mathbf{s}},\,t)=-\mu_{a,\lambda_F}I_{\lambda_F}(\mathbf{r},\,\hat{\mathbf{s}},\,t)-\mu_{s,\lambda_F}I_{\lambda_F}(\mathbf{r},\,\hat{\mathbf{s}},\,t)+\frac{\mu_{s,\lambda_F}}{4\pi}\int_{4\pi}I_{\lambda_F}(\mathbf{r},\,\hat{\mathbf{s}}_i,\,t)p_{\lambda_F}(\hat{\mathbf{s}}_i,\,\hat{\mathbf{s}})\mathrm{d}\omega_i+\frac{QY_{\lambda_x}\mu_{a,\lambda_{xF}}}{4\pi\tau_{\lambda_x}}\int_0^t\exp\left[-\left(\frac{t-t'}{\tau_{\lambda_x}}\right)\right]G_{\lambda_x}(\mathbf{r},\,t')\mathrm{d}t'. \tag{2}$$

The last term in Eq. (2) represents the fluorescence emission by the fluorophores; $G_{\lambda_x}(\mathbf{r},t)$ is the excitation light fluence at location $\mathbf{r}$ and time t and is defined as $G_{\lambda_x}(\mathbf{r},t)=\int_{4\pi}I_{\lambda_x}(\mathbf{r},\hat{\mathbf{s}},t)\mathrm{d}\omega$. The quantum yield of the fluorophores is denoted QY_{λ_x}, while $\mu_{a,\lambda_{xF}}$ is the absorption coefficient of the fluorophores at the excitation wavelength λ_x, and τ_{λ_x} denotes the lifetime of the fluorophores. Multiple fluorophores at a given location can be accounted for by modifying the source term appropriately. For example, the excitation fluence G_{λ_x} can be assumed to be distributed among these fluorophores in proportion to their absorption coefficients.

Finally, for both excitation and emission wavelengths, the Henyey–Greenstein phase function was used to account for the anisotropic nature of scattering by each layer of the skin and is expressed as

$$p_\lambda(\Theta) = \frac{1 - g_\lambda^2}{(1 + g_\lambda^2 - 2g_\lambda \cos\Theta)^{3/2}}, \quad (3)$$

where g_λ is the spectral scattering asymmetry factor and Θ is the angle between the incident direction $\hat{\mathbf{s}}_i$ and the scattering direction $\hat{\mathbf{s}}$.

C. Closure Laws

To solve the above equations, one needs (i) a model of the skin morphology, (ii) the optical and radiation characteristics c_λ or n_λ, $\mu_{a,\lambda}$, $\mu_{s,\lambda}$, and p_λ of each of the skin layers at both the excitation and the emission wavelengths, (iii) the spatial distribution of the fluorophores and (iv) their quantum yields QY_{λ_x}, (v) their lifetimes τ_{λ_x}, and (vi) their absorption coefficients $\mu_{a,\lambda_x F}$. Various optical models have been used to study light transport in skin [21,30,33], each varying in complexity. In the present study, the optical model of human skin developed by Tuchin [30] was chosen for its relative simplicity while capturing enough detail of the skin morphology. It consists of five plane-parallel layers, corresponding to (1) the epidermis, (2) the dermis, (3) the dermis with *plexus superficialis*, (4) the dermis, and (5) the dermis with *plexus profundus*. The thicknesses and optical properties of these layers at wavelengths 337 and 577 nm are reproduced in Table 1. Furthermore, in spite of varying refractive indices within the skin, reflection and refraction effects at the interfaces between the skin layers are considered negligible, as the difference in refractive index between these layers is very small (see Table 1). Instead, only the speed of light, $c_\lambda = c_0/n_\lambda$, used in Eqs. (1) and (2) was varied in each layer. Had there been a larger change in the refractive indices between adjacent layers, then the RTE would have had to be solved in each layer separately with the appropriate boundary conditions. Moreover, the skin surface and the interfaces between the skin layers are inherently rough and could be accounted for in the simulations to explain their influence on the distribution of excitation and fluorescence light in skin [34]. However, as a first-order approximation, they are assumed to be optically smooth and plane parallel as is commonly done in the literature [8–11]. It should be noted that the effects of skin roughness can be accounted for using various models as done by Lu and co-workers [34].

Furthermore, the distribution of fluorophores in the skin was based on studies reported in the literature [22,35]. According to Gillies *et al*. [22], the fluorescence from skin when excited at a wavelength of 337 nm is mainly from collagen present in the dermis. Moreover, König and Riemann [35] also reported the presence of NADH in human skin in the epidermis at a depth of 50 μm from the surface. Therefore, a model of fluorophore distribution within the skin was developed in which the sources of fluorescence from the skin were NADH and collagen. Moreover, each layer in the skin had only one fluorophore with NADH in the epidermis (layer 1) and collagen in all the other layers. Their characteristics, namely, the quantum yield, the fluorescence lifetime, and the absorption coefficient were then obtained from the literature. Some simplifying assumptions were made in using reported values of the fluorescence lifetimes of NADH and collagen. Free NADH exhibits a fluorescence lifetime of around 0.4 ns but displays a lifetime of 1.0–3.0 ns when bound to proteins [2]. In the present study, an average lifetime of 1.5 ns was used to account for NADH fluorescence, as is done in the literature [13,14]. There have also been reports of the fluorescence lifetimes of collagen in various forms and from various tissues [2]. However, very few report the lifetimes of collagen from skin at various excitation and emission wavelengths. König and Riemann [35] report two lifetimes of collagen, namely, 0.2–0.4 and 0.4–2.5 ns in human skin at excitation wavelengths of 300 to 340 nm and emission wavelengths of 420 to

Table 1. Optical Properties in the Five- and Two-Layer Skin Models[a]

Layer	Thickness[b] (μm)	n_λ[b]		$\mu_{a,\lambda}$[b] (cm^{-1})		$\mu_{s,\lambda}$[b] (cm^{-1})		g_λ[b]		τ_{λ_x}[c] (ns)	$\mu_{a,\lambda_x F}$[c] (cm^{-1})	QY_{λ_x}[c]
		λ_x	λ_F	λ_x	λ_F	λ_x	λ_F	λ_x	λ_F	$\sim\lambda_x$	$\sim\lambda_x$	$\sim\lambda_x$
Five-layer model												
1. Epidermis	100	1.5	1.5	32	10.7	165	120	0.72	0.78	1.5	3.15	0.05
2. Dermis	200	1.4	1.4	23	3	227	205	0.72	0.78	5.2	0.9	0.3
3. Dermis with plexus superficialis	200	1.4	1.4	40	5.2	246	219	0.72	0.78	5.2	0.9	0.3
4. Dermis	900	1.4	1.4	23	3	227	205	0.72	0.78	5.2	0.9	0.3
5. Dermis with plexus profundus	600	1.4	1.4	46	6	253	225	0.72	0.78	5.2	0.9	0.3
Two-layer model												
1. Epidermis	100	1.5	1.5	32	10.7	165	120	0.72	0.78	1.5	3.15	0.05
2. Sensor	50	1.37	1.37	1.88	0.1	10	10	0.9	0.9	11.25	1.88	0.74
3. Dermis	1900	1.4	1.4	32	4	237	213	0.72	0.78	5.2	0.9	0.3

[a] λ_x = 337 nm and λ_F = 577 nm [14,30].
[b] Ref. 30.
[c] Ref. 14.

460 nm. On the other hand, Pitts and Mycek [36] report a long fluorescence lifetime, 5.3 ns, from human skin at an excitation wavelength of 337 nm and an emission wavelength of 460 nm. The authors attributed this lifetime to collagen in human skin. In the present study, a fluorescence lifetime of 5.2 ns at an excitation wavelength of 337 nm and emission wavelength of 577 nm was chosen. These values were used by Mycek and co-workers [13,14] for simulating transient fluorescent light transport in colon tissue. While fluorescence lifetimes of collagen in skin might be different from those in the colon, the values were chosen for the purpose of illustration. In addition, the quantum yields and absorption coefficients of NADH and collagen at around 337 and 577 nm were obtained from the literature [13,14].

It should be noted that there are other endogenous fluorophores present in the skin, such as lipofuscin, which is excited in the UV–visible region and emits at around 570–590 nm [35]. However, the main purpose of this study is to analyze the fluorescence from an implanted glucose sensor and the effect of the autofluorescence from skin in recovering the lifetimes of the sensor fluorophore. Therefore these fluorophores were neglected as a first-order approximation. Finally, the *in vitro* emission maxima of NADH and collagen when excited at 337 nm are close to 450 and 390 nm, respectively [2]. However, their fluorescence at 577 nm is studied here because properties of skin at that wavelength are readily available in the literature [30]. Moreover, there have also been numerical and experimental studies of the time-resolved fluorescence from colon tissue at an excitation wavelength of 337 nm and an emission wavelength of 550 $\pm$ 20 nm with NADH and collagen as the principal fluorophores [13,14]. This indicates that even though the emission maxima of NADH and collagen is different from 577 nm, their fluorescence can still be observed *in vivo* at 577 nm. The fact that their fluorescence is not maximum is also beneficial to a potential embedded glucose sensor whose fluorescence could be overshadowed by the skin autofluorescence.

Moreover, several simplifying assumptions are made to model the fluorescence from the embedded glucose sensor. The glucose sensor is assumed to be a homogeneous absorbing and scattering plane-parallel slab of thickness 50 μm with uniformly distributed fluorophores. The fluorophore is assumed to be 9[[*N*-methyl-*N*-(*o*-boronobenzyl) amino]methyl]-anthracene, whose fluorescence lifetimes change as a function of glucose concentration [6]. The mean fluorescence lifetime of this compound at an excitation wavelength of 370 nm and an emission wavelength of 420 nm is 11.25 ns at a glucose concentration of 5 mM [6], which is close to the normal blood glucose level of 5.55 mM [37]. The fluorophore layer is assigned optical properties from the fluorescence layer described in Ref. 4. Here the fluorophore was arbitrarily assigned a quantum yield and an absorption coefficient of fluorescein, while the scattering coefficient was determined by assuming that the layer was a translucent gel polymer largely composed of water. However, these parameters can vary depending on the polymer material and the fluorophore selected. Furthermore, the skin model was simplified considerably to reduce the computational time. In the new model, skin was assumed to be made up of only two layers, the epidermis and the dermis. While the optical properties of the epidermis were retained from the previous five-layer model, those of the dermis were obtained by averaging the optical properties of the layers below the epidermis in the previous model. For example, the average absorption coefficient at the excitation wavelength is given by $\mu_{a,\lambda_x} = \sum_{i=2}^{5} \mu_{a,\lambda_x i} t_i / \sum_{i=2}^{5} t_i$, where t_i is the thickness of each layer i (see Table 1). This can be justified by the fact that these properties do not vary significantly from one layer to another in the dermis. Table 1 lists the thickness and optical properties of the two-layer skin model along with those of the embedded sensor layer.

D. Boundary Conditions

It is assumed that an index-matching material such as an oil or gel has been applied to the surface between the optical probe and the skin as is done in some optical experiments on human skin [38]. Then the internal reflection at the interface of the skin and the probe can be ignored. Indeed, if there were no index-matching material applied, any photon coming from within the tissue and reaching the interface at an angle greater than the critical angle would be reflected back into the tissue. The critical angle is defined as $\theta_c = \arcsin(1/n_{\text{epi}})$, where n_{epi} is the refractive index of the epidermis.

Finally, the incident pulse at $z = 0.0$ is assumed to be Gaussian with a peak intensity I_0 at time $t = t_c$ and pulse width t_p. The intensity profile for a Gaussian beam can be expressed as [39]

$$I_i(t) = I_0 \exp\left[-4 \ln(2)\left(\frac{t - t_c}{t_p}\right)^2\right]. \tag{4}$$

The pulse width t_p was chosen to be 1.0 ns, $t_c/t_p = 3$, and $I_0 = 10.0$ W/m^2 sr. The intensity is typical of a collimated beam from a pulsed LED with a peak power of 1.0 mW shining on an area of about 1.0 cm^2.

E. Method of Solution

Equations (1) and (2) are solved by using the modified method of characteristics [23]. In brief, the excitation light intensity is split into two components, (i) the radiation scattered away from the collimated radiation and (ii) the remnant of the incident collimated beam intensity given by Eq. (4) after partial extinction by absorption and scattering along its path. After Eq. (1) is used to solve for the excitation intensity in the skin, the fluorescent light intensity is then solved by using Eq. (2) at a particular instant in time. The reader is referred to Refs. 23 and 24 for a detailed description of the solution procedure. Moreover, the integrals present in Eqs. (1) and (2) are computed by using a quadrature scheme. It is a combination of two

Gaussian quadratures consisting of 24 directions along with the associated weights and has been successfully used in radiation transport calculations for strongly forward scattering media such as skin [40]. Finally, the time-resolved hemispherical reflectance and the autofluorescence emerging from the skin are computed as follows and plotted as a function of time:

$$R(t) = 2\pi \int_{\pi/2}^{n} I_{\lambda_x}(0,\ \theta,\ t)\cos\theta \sin\theta \mathrm{d}\theta,$$

$$F(t) = 2\pi \int_{\pi/2}^{n} I_{\lambda_F}(0,\ \theta,\ t)\cos\theta \sin\theta \mathrm{d}\theta. \quad (5)$$

Note that these equations correspond to a hypothetical detector of point size whose field of view is the entire hemisphere. The integration limits in the above equation can be altered to account for the fact that devices like optical fibers or streak cameras have only a limited field of view.

Retrieval of Fluorescence Lifetimes: In time-resolved fluorescence experiments, one recovers the fluorescence lifetimes from the normalized time-resolved fluorescence decay by deconvoluting the instrument response function (IRF) from the measured fluorescence decay. The IRF represents the response of the instrument to a fluorophore with zero lifetime. As performed experimentally, a model decay can be fitted to the numerical hemispherical fluorescence decay by using the incident pulse as the IRF. The software Fluofit [25,26] programmed in MATLAB was used to fit the simulated fluorescence decay to a model of the form

$$F(t) = \sum_{i=1}^{n_f} A_i \exp(-t/\tau_i), \quad (6)$$

where A_i and τ_i are the amplitudes and lifetimes and n_f is the total number of lifetimes. The program makes use of a least-squares fit and the Nelder–Meade simplex algorithm for optimization. The goodness of the fit is evaluated by the χ^2 parameter, whose value should approach 1.0 for a good fit to data with added noise. For a decay without noise, the χ^2 value approaches 0 [41]. Moreover, the program also provides standard deviations of the fitted lifetimes.

The program was first validated against a fluorescence decay generated from a homogeneous distribution of three fluorophores with lifetimes of 1.5, 5.2, and 11.25 ns and associated amplitudes of 0.7, 0.2, and 0.1, respectively. The lifetimes and amplitudes recovered by using Fluofit were 1.53, 5.40, and 11.27 ns, and their corresponding amplitudes were 0.71, 0.19, and 0.10, respectively. The maximum relative errors in the lifetimes and amplitudes were less than 5%, while χ^2 was 0.32. This indicates that Fluofit can be used to recover fluorescence lifetimes from fluorescence decay data.

4. Results and Discussion

Three cases of time-resolved fluorescence from skin are simulated. The first simulates time-resolved autofluorescence of a five-layer skin model exposed to a pulse of collimated light. A grid size of $N_z = 201$ resulting in a numerically converged solution was used. The second and third cases simulate time-resolved fluorescence from a two-layer skin model with and without an implanted fluorescence sensor. A grid size of $N_z = 206$ resulting in a numerically converged solution was used. In both cases, this corresponded to a spatial resolution of 10 μm in the z direction. A time step of $t/(N_z - 1)c$ was chosen for all the simulations, where t was the thickness of skin and c corresponded to the speed of light in the layer with the lowest refractive index at both the excitation and the emission wavelengths. In all cases, the total computational time necessary to obtain the solution was around three weeks. The optical and radiation characteristics for these simulations are given in Table 1.

A. Time-Resolved Autofluorescence of Human Skin

1. Time-Resolved Hemispherical Reflectance and Fluorescence

Figure 2 shows the normalized hemispherical reflectance $R(t)$ and autofluorescence $F(t)$ from the five-layer skin model exposed to the excitation pulse described by Eq. (4). Both were normalized by dividing their values by their maxima, estimated at 1.35 W/m^2 and 4.22×10^{-3} W/m^2, respectively, and multiplying by 10^6. The peak value of 10^6 was chosen on the basis of experiments [42]. Figure 2 indicates that the shape of the normalized hemispherical reflectance is identical to the shape of the excitation pulse. The temporal profile as well as the magnitude of the reflectance depends on the separation between the detector and the source. As the distance between the source and the detector increases, the depth of skin probed increases. Moreover, the path length traveled by the photons increases, and as a result the

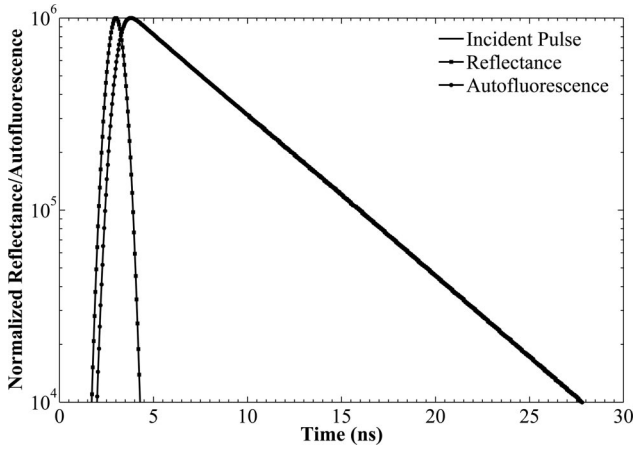

Fig. 2. Normalized hemispherical reflectance and autofluorescence at 577 nm from a five-layer skin model exposed to a collimated nanosecond pulse at 337 nm as a function of time.

temporal profile of the reflectance is broadened compared with the incident pulse [43]. However, the present study makes use of wide-beam illumination, and reflectance is measured at the center of this beam. Thus the detected reflectance represents an integrated contribution of the reflectances from all source–detector separations varying from zero to infinity. However, the major contribution to the diffuse reflectance is from photons backscattered by the topmost layers of the tissue. Since the path length traveled by these photons through the skin is negligible, the temporal profile of the reflectance does not undergo any broadening and is nearly identical to the incident pulse. Unlike the reflectance, the hemispherical autofluorescence is temporally broadened owing to the fluorescence lifetimes of the fluorophores.

The program Fluofit was then used to recover the fluorescence lifetime from fluorescence decays obtained by solving Eqs. (1) and (2), using a five-layer skin model. The recovered parameters τ_1 and τ_2 were 1.80 and 5.20 ns, while A_1 and A_2 were 0.02 and 0.98, respectively, with $\chi^2 = 0.06$. The recovered lifetime of 5.2 ns corresponds to the intrinsic lifetime of collagen used in the simulations. Moreover, several attempts were made to recover the fluorescence lifetimes from the simulated data. In all cases, the fluorescence lifetime of 5.2 ns was consistently recovered, unlike the input lifetime of NADH. This could be due to the fact that the contribution of NADH to the fluorescence was very minimal, making it difficult to numerically recover its lifetime.

2. *Reflectance and Autofluorescence from the Two-Layer Skin Model*

As described above, a two-layer skin model was also developed by averaging the properties of the five-layer skin model. The reflectance and autofluorescence from this skin model were computed. The peak values of reflectance and autofluorescence for the two-layer skin model were 1.25 W/m^2 and 3.35×10^{-3} W/m^2, respectively representing a decrease of 7% and 21% from the five-layer skin model. Moreover, as in the case of the five-layer model, the recovered lifetime of 5.20 ns was identical to the intrinsic lifetime of 5.20 ns of collagen used in the simulations. However, as before, the fluorescence lifetime of NADH could not be recovered. The χ^2 obtained was 0.94, indicating a good fit. A summary of the recovered lifetimes along with the standard deviations in the lifetimes output by Fluofit is presented in Table 2.

Therefore the two-layer model can be used for the feasibility analysis of the sensor for two reasons: (i) it yields the same magnitude of the fluorescence lifetimes of collagen as the five-layer model, and (ii) the computational time is reduced compared with the five-layer skin model. In addition, this confirms the advantage of time-resolved fluorescence measurements and contrasts with steady-state measurements, which are sensitive to the magnitude of the intensity. The magnitude is dependent on the optical properties, which in turn can be affected by uncertainties in the model parameters such as optical transport coefficients.

Table 2. Comparison of Input and Recovered Fluorescence Lifetimes of Normal Skin for Two-Layer Skin Model

Parameter	Actual Value (ns)	Recovered Value (ns)	Standard Deviation (ns)	χ^2
Without noise				
τ_1	1.5	0.81	1.56×10^{-5}	0.94
τ_2	5.2	5.20	7.05×10^{-8}	
With noise				
τ_1	1.5	1.27	1.81×10^{-5}	1.1
τ_2	5.2	5.20	8.98×10^{-7}	

B. Evaluation of an Embedded Glucose Sensor

There has been a rising interest in the use of implanted sensors for noninvasively monitoring concentrations of various analytes such as glucose in the human body. Several studies have reported the steady-state intensity and spatial distribution of fluorescence emission from hypothetical sensors under the skin by using the Monte Carlo method [3,4,44]. In the present study, simulations of time-resolved fluorescence from sensors embedded between the epidermis and the papillary dermis are presented for the first time to the best of our knowledge. The mean fluorescence lifetime of the fluorophore present in the sensor layer is varied from 11.25 to 12 ns in response to a change in the concentration of glucose in the interstitial fluid from 5 to 20 mM [6].

Figure 3 shows the time-resolved fluorescence of skin with this implanted sensor for these two glucose concentrations. Once again, Fluofit [25,26] was used to recover the fluorescence lifetimes from these decays. The recovered lifetimes, standard deviations, and χ^2 values for the two different glucose concentrations are reported in Table 3. For a glucose concentration of 5 mM, equivalent to 90 mg/dL, the recovered lifetimes were 0.03, 5.12, and 11.25 ns, and

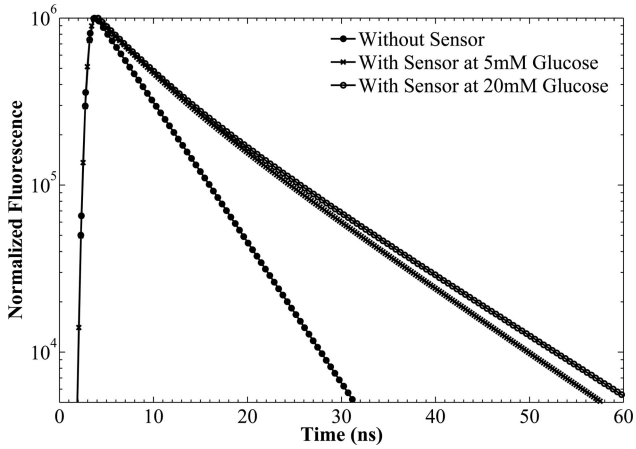

Fig. 3. Normalized hemispherical fluorescence at 577 nm from a two-layer skin model with an implanted glucose sensor, exposed to a collimated nanosecond pulse at 337 nm as a function of time.

Table 3. Comparison of Input and Recovered Lifetimes from a Two-Layer Skin Model

Glucose Concentration	Parameter	Actual Value (ns)	Recovered Value (ns)	Standard Deviation (ns)	χ^2
5 mM					
Without noise	τ_1	1.5	0.03	1.33×10^{-7}	0.05
	τ_2	5.2	5.12	3.54×10^{-6}	
	τ_3	11.25	11.25	2.31×10^{-6}	
With noise	τ_1	1.5	0.06	2.95×10^{-7}	1.35
	τ_2	5.2	5.07	8.94×10^{-6}	
	τ_3	11.25	11.18	5.11×10^{-6}	
20 mM					
Without noise	τ_1	1.5	0.13	5.97×10^{-7}	0.06
	τ_2	5.2	5.13	1.00×10^{-6}	
	τ_3	12.00	11.98	2.13×10^{-6}	
With noise	τ_1	1.5	0.03	6.95×10^{-7}	1.07
	τ_2	5.2	5.06	1.18×10^{-5}	
	τ_3	12.00	11.89	1.20×10^{-5}	

their corresponding amplitudes were 0.22, 0.35, and 0.42, respectively, while the χ^2 was 0.05. These lifetimes should be compared with the fluorescence lifetimes of the fluorophores used in the simulations, namely, 1.5, 5.2, and 11.25 ns.

Similarly, for a glucose concentration of 20 mM, the recovered lifetimes were 0.13, 5.13, and 11.98 ns with the corresponding amplitudes being 0.03, 0.46, and 0.51, respectively, and a χ^2 of 0.06. The lifetimes of the fluorophores used in the simulations were 1.5, 5.2, and 12.0 ns. Therefore, for both glucose concentrations, while the fluorescence lifetimes for collagen and the glucose sensor were recovered to within 1.3% of their input values used in the simulations, the lifetime of NADH in the epidermis could not be recovered. Moreover, the glucose concentrations corresponding to the recovered lifetimes in the two cases are 5 and 17.3 mM, respectively. This corresponds to a maximum error of 13.5% in the measurement of glucose concentration from such a time-resolved fluroescence sensor. These results suggest that it might be possible to measure glucose concentrations *in vivo* by using a time-resolved fluorescence sensor.

However, it should be noted that these simulations represent ideal conditions, which might not be achievable in actual experiments. For example, the morphology of skin changes from one person to another. This is especially important in diabetic patients, whose skin may thicken as a result of the disease [45]. In addition, time-resolved fluorescence measurement data are noisy. This aspect of the method is investigated in the following subsection.

C. Recovery of Fluorescence Lifetimes after Adding Noise to Numerical Data

The nature of the noise depends on the type of experimental setup used to measure the fluorescence lifetimes. For example, in time-correlated single-photon-counting experiments, the noise is Poissonian in nature [7]. In the present study, the numerical decay and IRF were normalized such that the peak value was set to 10^6 counts. Poissonian noise was then added to the generated curves by using the built in function "poissnrnd" in MATLAB. Furthermore, light detectors such as photomultiplier tubes have cutoffs below which they cannot distinguish a signal from noise. This effect was accounted for in the simulations by imposing a constant Poisson noise with a mean and variance of 10. As before, the peak value of 10^6 and the noise levels of 10 were chosen on the basis of our experiments [42].

Figure 4 shows a representative plot of the fluorescence decay after adding Poissonian noise along with the residuals. Note that the noise in the fluorescence is visible only at the initial times around 0 ns and not later owing to the scale of the plot, as is the case in experiments. The program Fluofit was then used to recover the fluorescence lifetimes from the data. A summary of the results obtained for the previously discussed cases is presented in Tables 2 and 3. In general, there was good agreement in the recovered lifetimes of collagen and the sensor (within 2.5%), while in all the cases the lifetime of NADH could not be recovered. Moreover, the χ^2 values were close to 0.0 and 1.0 for decays with and without noise, respectively, while the residuals were randomly distributed (Fig. 4), indicating good fits.

D. Recovery of NADH Lifetime

In all the above cases, it was found that the fluorescence lifetime of NADH could not be recovered. It was speculated that this could possibly be due to its very low concentration in the skin. To test this speculation, the quantum yield of NADH was arbitrarily set to 1.0 instead of 0.05, while all other input parameters were identical to the two-layer skin model without a sensor. No noise was added to the fluorescence decays. The recovered lifetimes were 1.50 and 5.2 ns, and the amplitudes were 0.30 and 0.70, respectively. The value of χ^2 was 0.11. These lifetimes are identical to the fluorescence lifetimes of NADH and collagen input in the simulations. This establishes that the

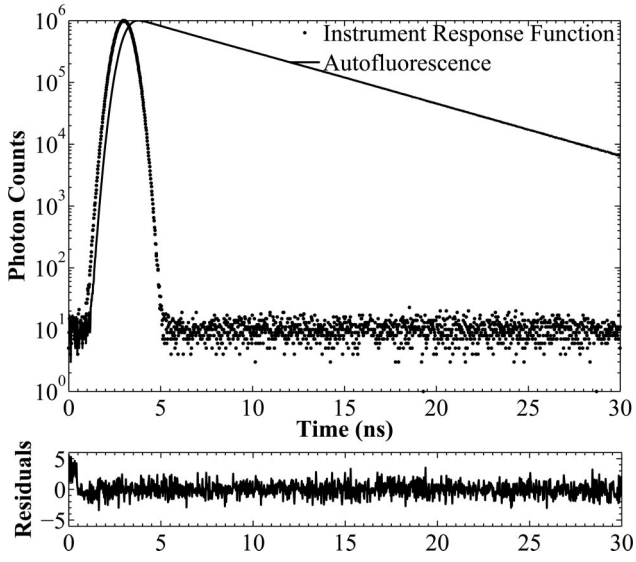

Fig. 4. Normalized hemispherical fluorescence at 577 nm from a two-layer skin model exposed to a collimated nanosecond pulse at 337 nm with added Poisson noise.

fluorescence lifetime of NADH could not be recovered in previous simulations because of the small contribution of NADH fluorescence to the overall fluorescence signal.

5. Conclusions

This paper presented simulations of time-resolved fluorescence from skin and their applications for designing implantable sensors for glucose monitoring. A five-layer skin fluorescence model was developed based on various data reported in the literature. The time-resolved fluorescence from human skin obtained by solving the radiative transfer equation was presented. A two-layer model of skin was also developed from the five-layer model by averaging the properties of the dermis. Finally, simulations of a sensor whose fluorescence lifetime depends on glucose concentration and which is implanted between the epidermis and the dermis were performed. In all cases the fluorophore lifetimes were retrieved from the simulated fluorescence decays by using Fluofit.

First, it was found that a two-layer model of skin composed of the epidermis and the dermis performed as well as a five-layer model of skin in terms of retrieving the fluorescence lifetimes. Second, the lifetime of NADH could not be retrieved in all the cases because of its negligible contribution to the fluorescence from the skin. On the other hand, the fluorescence lifetime of collagen could be recovered to within 2.5% with or without noise added to the simulated fluorescence decays. Moreover, the sensor lifetime was also recovered to within 1% with or without noise for glucose concentrations of 5 and 20 mM. Finally, the glucose concentrations were recovered to within 13.5% of their actual values.

The simulations in the present study are of particular interest for designing implantable fluorescence sensors, pharmacokinetics, and noninvasive diagnosis of various diseases that alter the autofluorescence properties of human skin. Further studies of time-resolved autofluorescence from skin could incorporate (i) more complex excitation and detection geometries, (ii) more complex skin morphology, (iii) and the presence of multiple fluorophores with complex spatial distributions. Moreover, simulations of time-resolved fluorescence from tissue can also be used to study diseases such as diabetes [46] and various cancers [13,14,47], which can affect the tissue fluorescence characteristics.

The authors thank Jörg Enderlein of Forschungszentrum Jülich, Germany, for his assistance in using the Fluofit program [25,26]. The authors also acknowledge the Diabetes Action Foundation for partially funding this research.

References

1. J. Pickup, F. Hussain, N. Evans, and N. Sachedina, "*In vivo* glucose monitoring: the clinical reality and the promise," Biosens. Bioelectron. **20,** 1897–902 (2005).
2. R. Richards-Kortum and E. Sevick-Muraca, "Quantitative optical spectroscopy for tissue diagnostics," Ann. Rev. Phys. Chem. **47,** 555–606 (1996).
3. M. McShane, S. Rastegar, and G. Cote, "Fluorescence-based implantable biosensors: Monte Carlo modeling for optical probe design," *Proceedings of the 20th Annual International Conference of the IEEE Engineering in Medicine and Biology Society* (IEEE, 1998), Vol. 4, pp. 1799–1802.
4. M. McShane, S. Rastegar, M. Pishko, and G. Cote, "Monte Carlo modeling for implantable fluorescent analyte sensors," IEEE Trans. Biomed. Eng. **47,** 624–632 (2000).
5. D. P. O'Neal, M. J. McShane, M. V. Pishko, and G. L. Cote, "Implantable biosensors: analysis of fluorescent light propagation through skin," Proc. SPIE **4263,** 20–24 (2001).
6. N. DiCesare and J. R. Lakowicz, "Evaluation of two synthetic glucose probes for fluorescence-lifetime-based sensing," Anal. Biochem. **294,** 154–160 (2001).
7. J. R. Lakowicz, *Principles of Fluorescence Spectroscopy* (Kluwer Academic/Plenum, 1999).
8. M. Keijzer, R. Richards-Kortum, S. Jacques, and M. Feld, "Fluorescence spectroscopy of turbid media: autofluorescence of the human aorta," Appl. Opt. **28,** 4286–4292 (1989).
9. I. V. Meglinski and D. Y. Churmakov, "A novel Monte Carlo method for the optical diagnostics of skin," Proc. SPIE **5141,** 133–141 (2003).
10. I. V. Meglinski, "Monte Carlo method in optical diagnostics of skin and skin tissues," Proc. SPIE **5254,** 30–43 (2003).
11. H. Zeng, C. E. MacAulay, B. Palcic, and D. I. McLean, "Monte Carlo modeling of tissue autofluorescence measurement and imaging," Proc. SPIE **2135,** 94–104 (1994).
12. K. Vishwanath, B. Pogue, and M.-A. Mycek, "Quantitative fluorescence lifetime spectroscopy in turbid media: comparison of theoretical, experimental and computational methods," Phys. Med. Biol. **47,** 3387–3405 (2002).
13. M.-A. Mycek, K. Vishwanath, B. W. Pogue, K. T. Schomacker, and N. S. Nishioka, "Simulations of time-resolved fluorescence in multilayered biological tissues: applications to clinical data modeling," Proc. SPIE **4958,** 51–59 (2003).
14. K. Vishwanath and M.-A. Mycek, "Do fluorescence decays remitted from tissues accurately reflect intrinsic fluorophore lifetimes?" Opt. Lett. **29,** 1512–1514 (2004).
15. M. S. Patterson and B. W. Pogue, "Mathematical model for time-resolved and frequency-domain fluorescence spectroscopy in biological tissues," Appl. Opt. **33,** 1963–1974 (1994).
16. M. A. O'Leary, D. A. Boas, X. D. Li, B. Chance, and A. G. Yodh, "Fluorescence lifetime imaging in turbid media," Opt. Lett. **21,** 158–160 (1996).
17. E. M. Sevick-Muraca and D. Y. Paithankar, "Imaging of fluorescence yield and lifetime from multiply scattered light re-emitted from random media," Proc. SPIE **2980,** 303–318 (1997).
18. D. Y. Paithankar, A. U. Chen, B. W. Pogue, M. S. Patterson, and E. M. Sevick-Muraca, "Imaging of fluorescent yield and lifetime from multiply scattered light reemitted from random media," Appl. Opt. **36,** 2260–2272 (1997).
19. A. H. Hielscher, R. E. Alcouffe, and R. L. Barbour, "Comparison of finite-difference transport and diffusion calculations for photon migration in homogeneous and heterogeneous tissues," Phys. Med. Biol. **43,** 1285–1302 (1998).
20. B. Chen, K. Stamnes, and J. J. Stamnes, "Validity of the diffusion approximation in bio-optical imaging," Appl. Opt. **40,** 6536–6366 (2001).
21. H. Zeng, C. MacAulay, D. I. McLean, and B. Palcic, "Reconstruction of *in vivo* skin autofluorescence spectrum from microscopic properties by Monte Carlo simulation," J. Photochem. Photobiol. B **38,** 234–240 (1997).
22. R. Gillies, G. Zonios, R. R. Anderson, and N. Kollias, "Fluorescence excitation spectroscopy provides information about human skin *in vivo,*" J. Investig. Dermatol. **115,** 704–707 (2000).
23. K. Katika and L. Pilon, "Modified method of characteristics

in transient radiative transfer," J. Quant. Spectrosc. Radiat. Transfer **98,** 220–237 (2006).
24. K. Katika and L. Pilon, "Steady-state directional diffuse reflectance and fluorescence of human skin," Appl. Opt. **45,** 4174–4183 (2006).
25. J. Enderlein and R. Erdmann, "Fast fitting of multi-exponential decay curves," Opt. Commun. **134,** 371–378 (1997).
26. "Fluofit—a MATLAB package for fitting multiexponential fluorescence decay curves," http://www.fz-juelich.de/ibi/ibi-1/enderlein/joerg/fluo/fluo.html, last accessed 22 December 2005.
27. A. Huntley and R. Drugge, "Anatomy of the skin, the electronic textbook of dermatology," http://www.telemedicine.org/stamford.htm, last accessed 5 February 2007.
28. I. V. Meglinski and S. J. Matcher, "Monte Carlo method in optical diagnostics of skin and skin tissues," Proc. SPIE **4241,** 78–87 (2001).
29. A. Krishnaswamy and G. V. G. Baranoski, *A Study on Skin Optics,* Technical Report CS-2004-01 (School of Computer Science, University of Waterloo, 2004).
30. V. Tuchin, ed., *Tissue Optics: Light Scattering Methods and Instruments for Medical Diagnosis* (SPIE, 2000).
31. M. F. Modest, *Radiative Heat Transfer* (Academic, 2002).
32. H. Quan and Z. Guo, "Fast 3-D optical imaging with transient fluorescence signals," Opt. Express **12,** 449–457 (2004).
33. D. Y. Churmakov, I. V. Meglinski, S. A. Piletsky, and D. A. Greenhalgh, "Skin fluorescence model based on the Monte Carlo technique," Proc. SPIE **5068,** 326–333 (2003).
34. J. Q. Lu, X.-H. Hu, and K. Dong, "Modeling of the rough-interface effect on a converging light beam propagating in a skin tissue phantom," Appl. Opt. **39,** 5890–5897 (2000).
35. K. König and I. Riemann, "High-resolution multiphoton tomography of human skin with subcellular spatial resolution and picosecond time resolution," J. Biomed. Opt. **8,** 432–439 (2003).
36. J. D. Pitts and M.-A. Mycek, "Design and development of a rapid acquisition laser-based fluorometer with simultaneous spectral and temporal resolution," Rev. Sci. Instrum. **72,** 3061–3072 (2001).
37. G. L. Cote, M. D. Fox, and R. B. Northrop, "Noninvasive optical polarimetric glucose sensing using a true phase measurement technique," IEEE Trans. Biomed. Eng. **39,** 752–756 (1992).
38. G. W. Hopkins and G. R. Mauze, "*In-vivo* NIR diffuse-reflectance tissue spectroscopy of human subjects," Proc. SPIE **3597,** 632–641 (1999).
39. C.-Y. Wu, "Propagation of scattered radiation in a participating planar medium with pulse irradiation," J. Quant. Spectrosc. Radiat. Transfer **64,** 537–548 (2000).
40. D. Baillis, L. Pilon, H. Randrianalisoa, R. Gomez, and R. Viskanta, "Measurements of radiation characteristics of fused quartz containing bubbles," J. Opt. Soc. Am. A **21,** 149–159 (2004).
41. J. Enderlein, "Comments on Fluofit and fitting fluorescence decay curves," Institute of Analytical Chemistry, Chemo- und Biosensors, University of Regensburg, PF 10 10 42, D-93040 Regensburg, Germany (personal communication, 2006).
42. K. M. Katika, L. Pilon, K. Dipple, S. Levin, J. Blackwell, and H. Berberoglu, "*In vivo* time-resolved autofluorescence measurements on human skin," Proc. SPIE **6078,** 60780L (2006).
43. A. Hielscher, S. Jacques, L. Wang, and F. Tittel, "The influence of boundary conditions on the accuracy of diffusion theory in time-resolved reflectance spectroscopy of biological tissues," Phys. Med. Biol. **40,** 1957–1975 (1995).
44. D. Y. Churmakov, I. V. Meglinski, and D. A. Greenhalgh, "Amending of fluorescence sensor signal localization in human skin by matching of the refractive index," J. Biomed. Opt. **9,** 339–346 (2004).
45. A. Huntley and R. Drugge, "Diabetes in skin disease. The electronic textbook of dermatology," http://www.telemedicine.org/dm/dmupdate.htm, last accessed 5 February 2007.
46. E. Hull, M. Ediger, A. Unione, E. Deemer, M. Stroman, and J. Baynes, "Noninvasive, optical detection of diabetes: model studies with porcine skin," Opt. Express **12,** 4496–4510 (2004).
47. R. Cubeddu, A. Pifferi, P. Taroni, A. Torricelli, G. Valentini, and E. Sorbellini, "Fluorescence lifetime imaging: an application to the detection of skin tumors," IEEE J. Sel. Top. Quantum Electron. **5,** 122–132 (1999).